Spatial solitons and stability in self-focusing and defocusing Kerr nonlinear media with generalized parity-time-symmetric Scarff-II potentials

Zhenya Yan,[1,2,*] Zichao Wen,[1] and Chao Hang[3,4]

[1]*Key Laboratory of Mathematics Mechanization, Institute of Systems Science, AMSS, Chinese Academy of Sciences, Beijing 100190, China*

[2]*State Key Laboratory of Theoretical Physics, Institute of Theoretical Physics, Chinese Academy of Sciences, Beijing 100190, China*

[3]*State Key Laboratory of Precision Spectroscopy and Department of Physics, East China Normal University, Shanghai 200062, China*

[4]*NYU-ECNU Institute of Physics at NYU Shanghai, Shanghai, 200062, China*

(Received 16 February 2015; revised manuscript received 18 May 2015; published 19 August 2015)

We present a unified theoretical study of the bright solitons governed by self-focusing and defocusing nonlinear Schrödinger (NLS) equations with generalized parity-time- ($\mathcal{PT}$) symmetric Scarff-II potentials. Particularly, a $\mathcal{PT}$-symmetric k-wave-number Scarff-II potential and a multiwell Scarff-II potential are considered, respectively. For the k-wave-number Scarff-II potential, the parameter space can be divided into different regions, corresponding to unbroken and broken $\mathcal{PT}$ symmetry and the bright solitons for self-focusing and defocusing Kerr nonlinearities. For the multiwell Scarff-II potential the bright solitons can be obtained by using a periodically space-modulated Kerr nonlinearity. The linear stability of bright solitons with $\mathcal{PT}$-symmetric k-wave-number and multiwell Scarff-II potentials is analyzed in detail using numerical simulations. Stable and unstable bright solitons are found in both regions of unbroken and broken $\mathcal{PT}$ symmetry due to the existence of the nonlinearity. Furthermore, the bright solitons in three-dimensional self-focusing and defocusing NLS equations with a generalized $\mathcal{PT}$-symmetric Scarff-II potential are explored. This may have potential applications in the field of optical information transmission and processing based on optical solitons in nonlinear dissipative but $\mathcal{PT}$-symmetric systems.

DOI: 10.1103/PhysRevE.92.022913 PACS number(s): 05.45.Yv, 42.65.Tg, 42.65.Wi, 11.30.Er

I. INTRODUCTION

The nonlinear Schrödinger (NLS) equation plays an important role in many fields of nonlinear physics [1–5]. The cubic NLS equation is shown to be completely integrable for both self-focusing and defocusing Kerr nonlinearities [6–8], which can be used to describe the propagation of optical pulses in Kerr-type optical media [3–5] or to describe the dynamics of matter waves in Bose-Einstein condensates, known as the Gross-Pitaevskii equation [9–12].

The NLS equations with real external potentials and gain-and-loss distributions have been studied in many works [13–17] because the refractive index of optical materials is usually complex, i.e., $n(x) = n_R(x) + in_I(x)$ with $n_R(x)$ and $n_I(x)$ being the real and imaginary parts, respectively. In optics, the propagation of a signal is stable unless the propagation constant of the light is in real spectrum range. This requirement can be efficiently achieved if the gain-and-loss distributions in the medium are exactly balanced to ensure the relation $n(x) = n^*(-x)$ [or $n_R(x) = n_R(-x)$ and $n_I(-x) = -n_I(x)$], which is known as the parity-time- ($\mathcal{PT}$) symmetric systems [18]. $\mathcal{PT}$ symmetry may exhibit entirely real spectrum of the respective optical potential in some parameter regions, referred to as the unbroken $\mathcal{PT}$ symmetry [18–20]. Beyond these regions, in the broken $\mathcal{PT}$ symmetry, the spectrum becomes complex and propagating waves may be either grow or decay.

Recently, various $\mathcal{PT}$-symmetric potentials have been introduced to the NLS equations, which have been shown to possess stable and unstable solitons of different types [21–38]. Examples include the NLS equations with $\mathcal{PT}$-symmetric Scarff-II potential [21–24,39], periodic potential [21,22,25,26], harmonic potential [27,28], Rosen-Morse potential [29], Gaussian potential [28,30,31], sextic anharmonic double-well potential [40], time-dependent harmonic-Gaussian potential [41], self-induced potential [42], etc. (see, e.g., Refs. [32–38]). One the other hand, due to the significant progress achieved in recent years on developing optical materials with adjustable refractive index, $\mathcal{PT}$-symmetric optical systems made of solid-state waveguides and fiber networks [43–45], multilevel atomic systems [46–50], and microcavities [51,52] have been suggested or realized experimentally. These practical systems provide a solid ground for the study of solitons in the NLS model with $\mathcal{PT}$-symmetric potentials.

The $\mathcal{PT}$-symmetric potentials play a key role in wave propagation in the NLS equations in fiber and waveguide optics. As an example, wave propagation with a $\mathcal{PT}$-symmetric Scarff-II potential in both linear and nonlinear models has been studied in recent years [21–24]. The $\mathcal{PT}$-symmetric Scarff-II potential can support stable bright solitons in the NLS models within particular parameter regions [19,20]. More importantly, the real and imaginary parts of the $\mathcal{PT}$-symmetric k-wave-number Scarff-II potential [19,53] both approach to zero as $|x| \to \infty$ [cf. Eq. (4), for $V_0 = 2$, $W_0 = 1$, $k = \sqrt{2}$, we have $V(x) \approx 3.25 \times 10^{-24}$ and $W(x) \approx 1.04 \times 10^{-12}$ as $x = 20$], that is, they have a limited effect on the nonlinear waves for the NLS equation only in a boundary region (e.g., $|x| < 20$ for $k = \sqrt{2}$) [cf. Eq. (3)] and can more easily support the existence of bright solitons in the NLS equation, compared with the $\mathcal{PT}$-symmetric harmonic and optical lattice potentials, which always have the effect on the nonlinear waves in the whole region (see, e.g., Refs. [21,22,25–28]). However, a complete analysis of the soliton stability in

*zyyan@mmrc.iss.ac.cn

a $\mathcal{PT}$-symmetric k-wave-number Scarff-II potential is still lacking in a full parameter space [e.g., the space consists of amplitudes of real and imaginary parts of the $\mathcal{PT}$-symmetric k-wave-number Scarff-II potential and the wave number k, see Eq. (4)]. In addition, the study of optical solitons could be very useful in information science. For example, one can use optical solitons in coding for secured optical communication, etc.

In this work we propose a unified study of optical bright solitons governed by self-focusing and defocusing NLS equations with generalized $\mathcal{PT}$-symmetric Scarff-II potentials. Particularly, we consider a $\mathcal{PT}$-symmetric k-wave-number Scarff-II potential and a multiwell Scarff-II potential, respectively. For the k-wave-number Scarf-II potential, we show that by using two k-wave-number rays and a k-wave-number parabola one can divide the parameter space $\{(V_0,W_0)|V_0 > 0, W_0 \in \mathbb{R}\}$ (V_0 and W_0 are, respectively, the real and imaginary parts of the potential) in different regions, corresponding to unbroken and broken $\mathcal{PT}$ symmetry and the bright solitons with self-focusing and defocusing Kerr nonlinearities. For the multiwell Scarff-II potential we obtain bright solitons by using a periodically space-modulated Kerr nonlinearity. Then we analyze the linear stability of bright solitons for both potentials in details by using numerical simulations. Surprisingly, stable and unstable bright solitons are found in both regions of unbroken and broken $\mathcal{PT}$ symmetry due to the existence of the nonlinearity. Furthermore, we explore the bright solitons in three-dimensional (3D) self-focusing and defocusing NLS equations with a generalized $\mathcal{PT}$-symmetric Scarff-II potential.

Turning to the possible experimental implementation of the models we will study [see Eq. (1) with $\mathcal{PT}$-symmetric k-wave-number and multiwell Scarff-II potentials (4) and (19)], we can exploit a $\mathcal{PT}$-symmetric refractive index profile (e.g., the considered $\mathcal{PT}$-symmetric k-wave-number Scarff-II potential) imprinted in a cold gas of two atomic isotopes of Λ-type configuration (say of ^{87}Rb and ^{85}Rb isotopes) loaded in an atomic cell, as suggested in Refs. [46–50]. By the interference of two Raman resonances, the required spatial distribution of the refractive index (i.e., the k-wave-number and multiwell Scarff-II potentials) can be achieved by a proper combination of a control laser field and a far-off-resonance Stark laser field. Since the refractive index of the atomic vapor is determined by two external laser fields, whose intensities can be lowered to several microwatts achievable for the lasers nowadays, the system has the advantages of real-time all-optical tunable capability and controllable $\mathcal{PT}$-symmetry accuracy. In addition, the studied model supports a large Kerr nonlinearity (which is at least 10^{13}-order larger than those measured for usual nonlinear optical materials) due to the Raman resonant character, which favors the formation of optical bright solitons.

The rest of this paper is arranged as follows. Section II gives the bright spatial solitons in one-dimensional $\mathcal{PT}$-symmetric potentials. Both $\mathcal{PT}$-symmetric k-wave-number and multiwell Scarff-II potentials are considered. The linear stability of optical bright solitons is analyzed. Stable solitons are found for both unbroken and broken $\mathcal{PT}$-symmetric potentials. Section III gives the bright solitons in 3D self-focusing and defocusing NLS equations with a generalized $\mathcal{PT}$-symmetric Scarff-II potential. Finally, the last section contains a summary of main results obtained in this work.

II. BRIGHT SOLITONS IN ONE-DIMENSIONAL $\mathcal{PT}$-SYMMETRIC POTENTIALS

A. Nonlinear physical model and stationary solutions

Now we uniformly investigate the exact localized solution modes and their stabilities of self-focusing and defocusing NLS equations with a $\mathcal{PT}$-symmetric potential. In the dimensionless form, the physical model can be written as [21]

$$i\partial_t\psi + \partial_x^2\psi + [V(x) + iW(x)]\psi + g|\psi|^2\psi = 0, \quad (1)$$

where $\partial_t = \partial/\partial t$, $\partial_x = \partial/\partial x$, $\psi \equiv \psi(x,t)$ is a complex field of x,t (x and t are, respectively, dimensionless space and time), $V(x)$ is a real external potential, $W(x)$ is a real gain-and-loss distribution, and g characterizes the self-focusing ($g > 0$) or defocusing ($g < 0$) Kerr nonlinearity, respectively. Equation (1) is associated with a variational principle $\delta\mathcal{L}(\psi)/\delta\Psi^* = 0$ with the Lagrangian density

$$\mathcal{L}(\psi) = i(\psi^*\psi_t - \psi\psi_t^*) + 2|\psi_x|^2 + 2[V(x) + iW(x)]|\psi|^2 + g|\psi|^4. \quad (2)$$

The $\mathcal{PT}$-symmetric potential $V(x) + iW(x)$ leads to the sufficient (but not necessary) condition $V(x) = V(-x)$ and $W(x) = -W(-x)$. The quasipower and power of Eq. (1) are given by $Q(t) = \int_{-\infty}^{+\infty}\psi(x,t)\psi^*(-x,t)dx$ and $P(t) = \int_{-\infty}^{+\infty}|\psi(x,t)|^2dx$, respectively. One can readily get that $Q_t = i\int_{-\infty}^{+\infty} g\psi(x,t)\psi^*(-x,t)[|\psi(x,t)|^2 - |\psi(-x,t)|^2]dx$ and $P_t = -2\int_{-\infty}^{+\infty} W(x)|\psi(x,t)|^2dx$. Note that if we set $t \to z$ in Eq. (1), where z denotes the propagation distance [21], then the following results about Eq. (1) still hold as $t \to z$.

We focus on the stationary solutions of Eq. (1) in the form $\psi(x,t) = \phi(x)e^{i\mu t}$, where μ is the real propagation constant and the complex function $\phi(x)$ satisfies the stationary NLS equation with varying parameter modulation:

$$\mu\phi(x) = \frac{d^2\phi(x)}{dx^2} + [V(x) + iW(x)]\phi(x) + g|\phi(x)|^2\phi(x), \quad (3)$$

which can be solved by using numerical methods.

In the following, we consider two different types of $\mathcal{PT}$-symmetric potential, i.e., the $\mathcal{PT}$-symmetric k-wave-number Scarff-II potential and the periodically space-modulated Scarff-II potential, and study the exact localized solutions and their linear stability in both regions of unbroken and broken $\mathcal{PT}$ symmetry.

B. $\mathcal{PT}$-symmetric k-wave-number Scarff-II potential

To study the soliton solutions of Eq. (3), we first consider the $\mathcal{PT}$-symmetric k-wave-number Scarff-II potential [19,53], which is given as

$$V(x) = V_0\,\mathrm{sech}^2(kx), \quad W(x) = W_0\,\mathrm{sech}(kx)\tanh(kx), \quad (4)$$

where $k > 0$ denotes the wave number and $V_0 > 0$ and W_0 are real parameters and modulate amplitudes of the external potential and gain-and-loss distribution, respectively. The wave number k and amplitude V_0 can modulated the well width and depth of the potential $V(x)$, respectively. W_0 can modulate

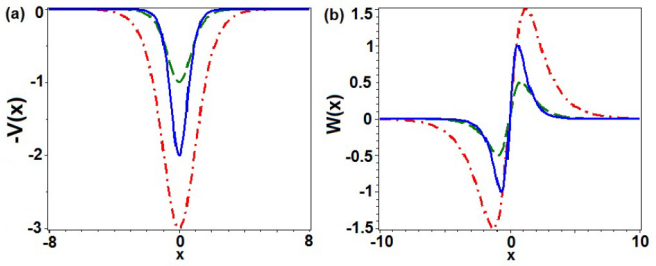

FIG. 1. (Color online) Real (a) and imaginary (b) parts of $\mathcal{PT}$-symmetric k-wave-number Scarff-II potential (4). (a) $V_0 = 3, k = 1/\sqrt{2}$ (dashed-dotted line), $V_0 = 2, k = \sqrt{2}$ (solid line), $V_0 = k = 1$ (dashed line) and (b) $W_0 = 3, k = 1/\sqrt{2}$ (dashed-dotted line), $W_0 = 2, k = \sqrt{2}$ (solid line), $W_0 = k = 1$ (dashed line).

the impact of the gain-and-loss distribution. For the case $k = 1$, the $\mathcal{PT}$-symmetric k-wave-number Scarff-II potential (4) becomes the usual $\mathcal{PT}$-symmetric Scarff-II potential [19]. Figure 1 displays the $\mathcal{PT}$-symmetric k-wave-number Scarff-II potential (4) for different amplitudes V_0, W_0, and wave number k.

It follows from Eq. (4) that $V(x), W(x) \to 0$ as $|x| \to \infty$ and/or $k \to \infty$ and $V(x) \to V_0, W(x) \to 0$ as $x = 0$ and/or $k \to 0$. If $V_0 W_0 \neq 0$, then $V(x)$ and $W(x)$ satisfy the family of elliptic curves:

$$\left[\frac{V(x)}{V_0} - \frac{1}{2}\right]^2 + \frac{W^2(x)}{W_0^2} = \frac{1}{4} \tag{5}$$

with the centers being $(V_0/2,0)$ in the $(V(x), W(x))$ space. It is easy to see that the family of elliptic curves is dependent on the wave number k.

In general, for the $\mathcal{PT}$-symmetric k-wave-number Scarff-II potential $S_{\mathcal{PT}} = V(x) + iW(x)$ with $V(x)$ and $W(x)$ given by Eq. (4) for any real parameters V_0, W_0 there are the following three cases:

(i) When $W_0 = 0$, the potential $S_{\mathcal{PT}} = V(x)$ is a real, Hermitian, and $\mathcal{PT}$-symmetric potential;

(ii) when $V_0 = 0$, the potential $S_{\mathcal{PT}} = iW(x)$ is a pure imaginary, non-Hermitian, and $\mathcal{PT}$-symmetric potential; and

(iii) when $V_0 W_0 \neq 0$, the potential $S_{\mathcal{PT}} = V(x) + iW(x)$ is a complex, non-Hermitian, and $\mathcal{PT}$-symmetric potential.

In the following, we mainly consider the potential $S_{\mathcal{PT}} = V(x) + iW(x)$ in Case (iii) with $V_0 > 0$.

1. Linear eigenvalue problem with unbrokon and broken $\mathcal{PT}$ symmetry

The linear eigenvalue problem

$$L_{\mathcal{PT}}\Phi(x) = \lambda\Phi(x), \quad L_{\mathcal{PT}} = -\partial_x^2 - [V(x) + iW(x)] \tag{6}$$

with $V(x)$ and $W(x)$ given by Eq. (4) exhibits an entirely real spectrum provided that two amplitudes $V_0 > 0, W_0$ and the wave number k satisfy

$$|W_0| \leqslant V_0 + \frac{k^2}{4}, \tag{7}$$

where λ and $\Phi(x)$ are eigenvalue and eigenfunction, respectively. The inequality (7) is called the $\mathcal{PT}$-symmetry-unbreaking condition. If $|W_0| > V_0 + k^2/4$, then the spectrum

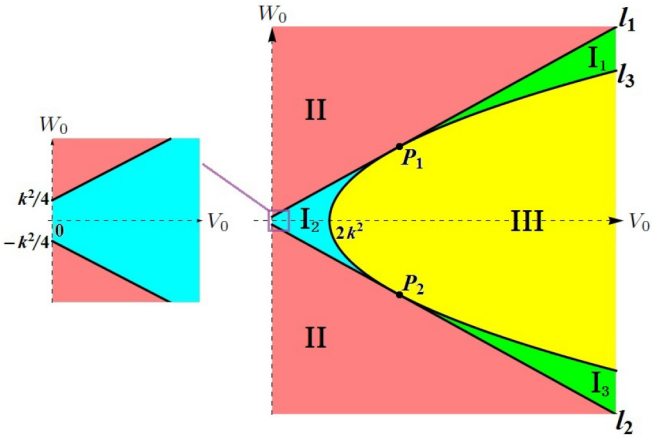

FIG. 2. (Color online) The parameter space $\{(V_0, W_0)|V_0 > 0, W_0 \in \mathbb{R}\}$ can be divided into different regions by two families of k-wave-number open rays $l_{1,2}$: $W_0 = \pm(V_0 + k^2/4)$ with $V_0 > 0$ and a family of k-wave-number parabola l_3: $W_0^2 = 9k^2(V_0 - 2k^2)$, corresponding to unbroken and broken $\mathcal{PT}$ symmetry and bright solitons with self-focusing ($g > 0$) and defocusing ($g < 0$) Kerr nonlinearities. The tangent points of three curves are $P_{1,2} = (17k^2/4, \pm 9k^2/2)$.

becomes complex. For $k = 1$, the condition (7) reduces to the well-known one, $|W_0| \leqslant V_0 + 1/4$ [19,20]. Therefore, two families of k-wave-number open rays l_1:

$$W_0 = V_0 + k^2/4, \quad V_0 > 0 \tag{8}$$

and l_2:

$$W_0 = -(V_0 + k^2/4), \quad V_0 > 0 \tag{9}$$

divide the parameter space $\{(V_0, W_0)|V_0 > 0, W_0 \in \mathbb{R}\}$ into two regions, i.e., the unbroken $\mathcal{PT}$-symmetric region $|W_0| \leqslant V_0 + k^2/4$ and the broken $\mathcal{PT}$-symmetric region $|W_0| > V_0 + k^2/4$ (see Fig. 2).

2. The conditions for the existence of nonlinear modes

For the given $\mathcal{PT}$-symmetric k-wave-number Scarff-II potential (4) with $V_0 > 0$ and $W_0 \in \mathbb{R}$, Eq. (3) admits the unified bright soliton for both self-focusing ($g > 0$) and defocusing ($g < 0$) nonlinearities

$$\phi(x) = \sqrt{\frac{1}{g}\left(\frac{W_0^2}{9k^2} - V_0 + 2k^2\right)}\,\mathrm{sech}(kx)e^{i\varphi(x)}, \tag{10}$$

where $\mu = k^2$, $g[W_0^2/(9k^2) - V_0 + 2k^2] > 0$, and the phase is

$$\varphi(x) = \frac{W_0}{3k^2}\arctan[\sinh(kx)]. \tag{11}$$

In particular, when $g = k = 1$ or $-g = k = 1$, the solution (10) reduces to the known ones as given in Refs. [21,24].

Now we analyze the conditions for the existence of bright soliton (10) for parameters W_0, V_0, k, and g. For the positive (self-focusing) nonlinearity $g > 0$, the condition for the existence of bright soliton (10) is given by

$$W_0^2 > 9k^2(V_0 - 2k^2). \tag{12}$$

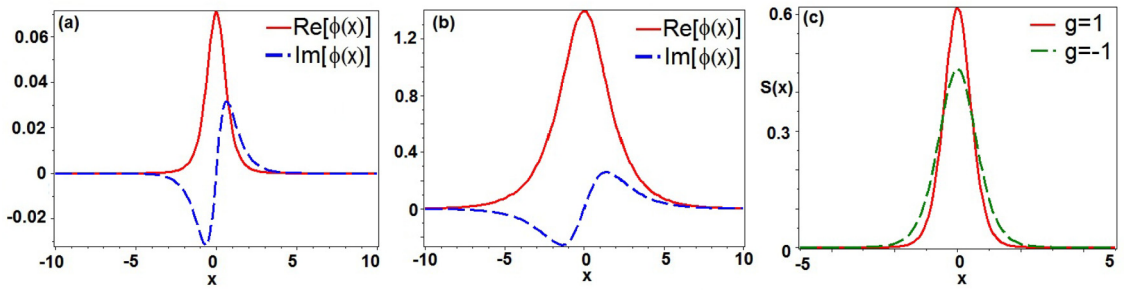

FIG. 3. (Color online) Real (solid lines) and imaginary (dashed lines) parts of bright soliton (10) for (a) the self-focusing nonlinearity $g = 1$ with $V_0 = 5$, $W_0 = 5.2$, $k = \sqrt{2}$ and (b) defocusing nonlinearity $g = -1$ with $V_0 = 3$, $W_0 = 0.5$, $k = 1/\sqrt{2}$. (c) The transverse power-flow vector (Poynting vector) $S(x)$ given by Eq. (16) for the self-focusing nonlinearity $g = 1$ with $V_0 = 5$, $W_0 = 5.2$, $k = \sqrt{2}$ (solid line) and defocusing nonlinearity $g = -1$ with $V_0 = 3$, $W_0 = 0.5$, $k = 1/\sqrt{2}$ (dashed line).

The real and imaginary parts of the soliton are displayed in Fig. 3(a). For the negative (defocusing) nonlinearity $g < 0$, the condition for the existence of bright soliton (10) is given by

$$|W_0| < 3k\sqrt{V_0 - 2k^2}, \quad V_0 > 2k^2. \tag{13}$$

The real and imaginary parts of the soliton are illustrated in Fig. 3(b).

Taking into account the conditions (12) and (13) for the existence of bright soliton (10) for $g > 0$ and $g < 0$, the parameter space $\{(V_0, W_0)|V_0 > 0, W_0 \in \mathbb{R}\}$ can be divided into another two fundamental regions by the family of parabolas l_3: $W_0^2 = 9k^2(V_0 - 2k^2)$ with the vertex being $(2k^2, 0)$. These two conditions (12) and (13) for bright solitons with $g > 0$ and $g < 0$, respectively, are shown in Fig. 2.

Note that the bright soliton (10) with $g > 0$ [attractive case for Eq. (1)] can also exist for the region $\{(V_0, W_0)|V_0 \leqslant 0, W_0 \in \mathbb{R}\}$.

Two branches of k-wave-number open rays $l_{1,2}$ given by Eqs. (8) snd (9) are tangent to the parabola l_3:

$$W_0^2 = 9k^2(V_0 - 2k^2) \tag{14}$$

at the points $P_{1,2} = (17k^2/4, \pm 9k^2/2)$, respectively. In other words, $|V_0 + k^2/4| > 3k\sqrt{V_0 - 2k^2}$ always holds except for two tangent points $P_{1,2}$, at which they are equal (see Fig. 2 and Ref. [54] for details).

Therefore, the parameter space $\{(V_0, W_0)|V_0 > 0, W_0 \in \mathbb{R}\}$ can be divided into eight regions, i.e.,

$$\begin{aligned}&\{(V_0, W_0)|V_0 > 0, W_0 \in \mathbb{R}\}\\ &\quad = \mathrm{I}_1 + \mathrm{I}_2 + \mathrm{I}_3 + \mathrm{II} + \mathrm{III} + l_1 + l_2 + l_3,\end{aligned} \tag{15}$$

where "+" denotes the union of two sets, these regions $\mathrm{I}_{1,2,3}$, II, III denote open sets without the corresponding boundaries (see Fig. 2). To make it become clearer, we summarize these different regions in Table I. One can see that the region for bright solitons with self-focusing nonlinearity contains both regions for unbroken and broken $\mathcal{PT}$ symmetry, whereas the region for bright solitons with defocusing nonlinearity contains only the region for unbroken $\mathcal{PT}$ symmetry.

For any complex solution $\phi(x) = |\phi(x)|e^{i\varphi(x)}$ with $\varphi(x)$ bering a real phase of $\phi(x)$, we find that its corresponding transverse power-flow or Poynting vector and the gradient of phase obey the relation $S(x) = \frac{i}{2}(\phi\phi_x^* - \phi^*\phi_x) = |\phi(x)|^2\varphi_x$. For the bright soliton (10), its corresponding transverse power-flow or "Poynting vector" is given by

$$S(x) = \frac{W_0}{3kg}\left(\frac{W_0^2}{9k^2} - V_0 + 2k^2\right)\mathrm{sech}^3(kx), \tag{16}$$

which implies that $\mathrm{sgn}(S(x)) = \mathrm{sgn}(W_0)$ for any x and $g = \pm 1$ [see Fig. 3(c)] since $k > 0$ and $g[W_0^2/(9k^2) - V_0 + 2k^2] > 0$ are required for the conditions of the existence of bright solitons. Therefore, the power always flows in one direction, i.e., from the gain toward the loss. In addition, we have the conserved power related to solution (10) is $P(t) = \frac{2}{gk}(\frac{W_0^2}{9k^2} - V_0 + 2k^2)$.

3. *Stability of nonlinear modes*

Next we study the linear stability of the bright solitons (10) in the above-mentioned different regions. To this end, we considered a perturbed bright soliton solution [55]

$$\psi(x,t) = \{\phi(x) + \epsilon[F(x)e^{i\delta t} + G^*(x)e^{-i\delta^* t}]\}e^{i\mu t}, \tag{17}$$

TABLE I. The regions for unbroken and broken $\mathcal{PT}$ symmetry and the existence of bright solitons with self-focusing ($g > 0$) and defocusing ($g < 0$) nonlinearities in the parameter space $\{(V_0, W_0)|V_0 > 0, W_0 \in \mathbb{R}\}$ [Yes and No denote the corresponding problems exist and do not exist in the regions, respectively. The signs + and − denote the union and difference of two sets, respectively].

Region	Linear problem ($g = 0$): unbroken $\mathcal{PT}$ symmetry	Linear problem ($g = 0$): broken $\mathcal{PT}$ symmetry	Nonlinear problem ($g > 0$): soliton (10)	Nonlinear problem ($g < 0$): soliton (10)
$\mathrm{I}_1 + \mathrm{I}_2 + \mathrm{I}_3 + l_1 + l_2 - \{P_{1,2}\}$	Yes	No	Yes	No
l_3	Yes	No	No	No
II	No	Yes	Yes	No
III	Yes	No	No	Yes

where $\phi(x)e^{i\mu t}$ is a stationary solution of Eq. (1), $\epsilon \ll 1$, and $F(x)$ and $G(x)$ are the eigenfunctions of the linearized eigenvalue problem. Substituting Eq. (17) in Eq. (1) and linearizing with respect to ϵ, we obtain the following linear eigenvalue problem:

$$\begin{bmatrix} L & g\phi^2(x) \\ -g\phi^{*2}(x) & -L^* \end{bmatrix}\begin{bmatrix} F(x) \\ G(x) \end{bmatrix} = \delta\begin{bmatrix} F(x) \\ G(x) \end{bmatrix}, \qquad (18)$$

where $L = \partial_x^2 + V(x) + iW(x) + 2g|\phi(x)|^2 - \mu$.

The stability of the perturbed soliton $\psi(x,t)$ is related to the imaginary parts $\mathrm{Im}(\delta)$ of all eigenvalues δ. If $|\mathrm{Im}(\delta)| > 0$, then the solution $\psi(x,t)$ will grow exponentially with t (i.e., it is unstable), otherwise the solution $\psi(x,t)$ is stable. In the following, we study the stability of exact soliton (10) under an initial random noise perturbation up to 2% of its amplitude for different parameters.

Since the regions I_1 and I_3 are symmetric about the V_0 axes, we only need to consider one of them (say I_1). Thus we leave four regions for studying the linear stability of the bright solitons (10). The regions I_1, I_2, and II correspond to bright solitons for the self-focusing nonlinearity $g = 1$, whereas the region III corresponds to bright solitons for the defocusing nonlinearity $g = -1$. To be specific, we study the stability of bright solitons in the regions for unbroken and broken $\mathcal{PT}$ symmetry with $k = 1$ (the usual $\mathcal{PT}$-symmetric Scarff-II potential) and $k \neq 1$. Note that we only consider $W_0 > 0$ as $W(x)$ is an odd function.

If $k = 1$ and $g = 1$: (i) for $V_0 = 0.1$, $W_0 = 0.5$ in region II (broken $\mathcal{PT}$ symmetry), we numerically obtain the spectrum of eigenvalues δ [see Fig. 4(a)] and a stable propagation of the soliton intensity $|\psi(x,t)|^2$ shown in Fig. 4(b); (ii) for $V_0 = 1.5$, $W_0 = 0.2$ in region I_2 (unbroken $\mathcal{PT}$ symmetry), we numerically obtain the spectrum of eigenvalues δ [see Fig. 4(c)] and a stable propagation of the soliton intensity $|\psi(x,t)|^2$ shown in Fig. 4(d); (iii) for $V_0 = 5$, $W_0 = 5.2$ in region I_1 (unbroken $\mathcal{PT}$ symmetry), we numerically obtain the spectrum of eigenvalues δ [see Fig. 4(e)] and an unstable propagation of the soliton intensity $|\psi(x,t)|^2$ shown in Fig. 4(f); (iv) for $V_0 = -0.1$, $W_0 = 0.1$ in region $\{(V_0, W_0)|V_0 \leqslant 0, W_0 \in \mathbb{R}\}$, we numerically obtain the spectrum of eigenvalues δ [see Fig. 4(g)] and an unstable propagation of the soliton intensity $|\psi(x,t)|^2$ shown in Fig. 4(h). If $k = 1$ and $g = -1$, for $V_0 = 3$, $W_0 = 0.5$ in the region III (unbroken $\mathcal{PT}$ symmetry), we numerically obtain the spectrum of eigenvalues δ [see Fig. 5(a)] and a stable propagation of the soliton intensity $|\psi(x,t)|^2$ shown in Fig. 5(b). We stress that the stability (instability) of the bright solitons in the broken (unbroken) $\mathcal{PT}$-symmetry region is due to the existence of Kerr nonlinearity.

If $k \neq 1$ and $g = 1$: (i) for $V_0 = 0.05$, $W_0 = 0.25$, $k = 1/\sqrt{2}$ in region II (broken $\mathcal{PT}$ symmetry), we numerically obtain the spectrum of eigenvalues δ [see Fig. 6(a)] and a stable propagation of the soliton intensity $|\psi(x,t)|^2$ shown in Fig. 6(b); (ii) for $V_0 = 2.16$, $W_0 = 0.12$, $k = \sqrt{1.2}$ in region I_2 (unbroken $\mathcal{PT}$ symmetry), we numerically obtain the spectrum of eigenvalues δ [see Fig. 6(c)] and a stable propagation of the soliton intensity $|\psi(x,t)|^2$ shown in Fig. 6(d); (iii) for $V_0 = 10$, $W_0 = 10.4$, $k = \sqrt{2}$ in region I_1 (unbroken $\mathcal{PT}$ symmetry), we numerically obtain the spectrum of

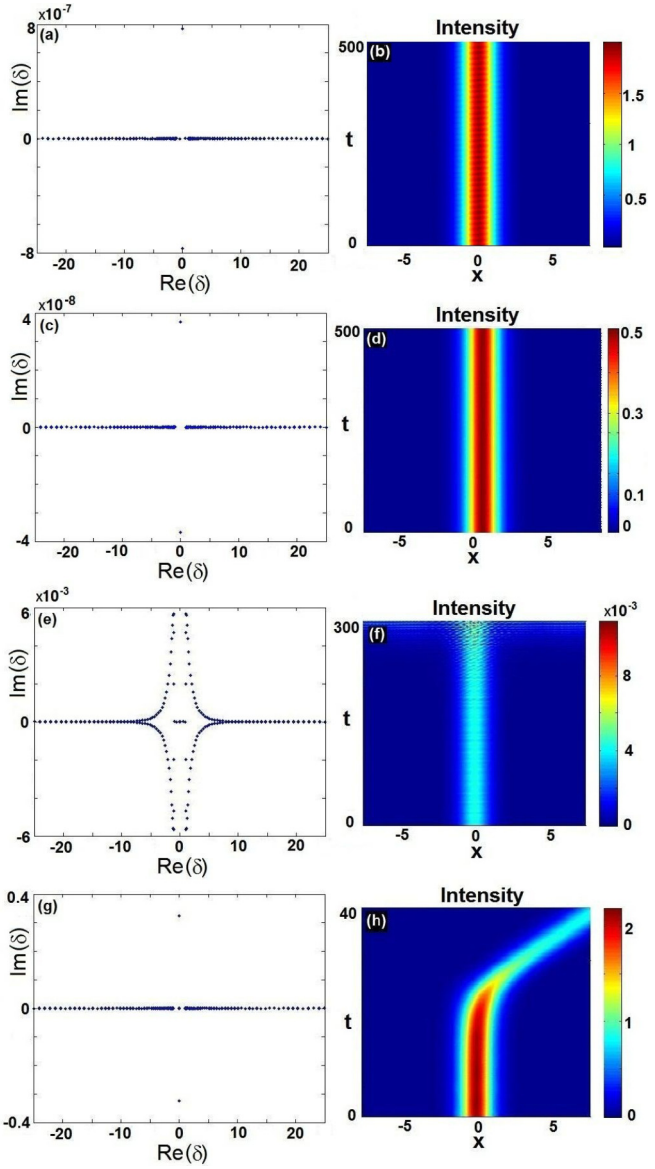

FIG. 4. (Color online) The linear stability eigenvalues (left column) and propagation of soliton intensity $|\psi(x,t)|^2$ with $g = k = 1$ (right column). [(a) and (b)] $V_0 = 0.1$, $W_0 = 0.5$ (in the region II), [(c) and (d)] $V_0 = 1.5$, $W_0 = 0.2$ (in the region I_2), [(e) and (f)] $V_0 = 5$, $W_0 = 5.2$ (in the region I_1), and [(g) and (h)] $V_0 = -0.1$, $W_0 = 0.1$ (in the region $\{(V_0, W_0)|V_0 \leqslant 0, W_0 \in \mathbb{R}\}$).

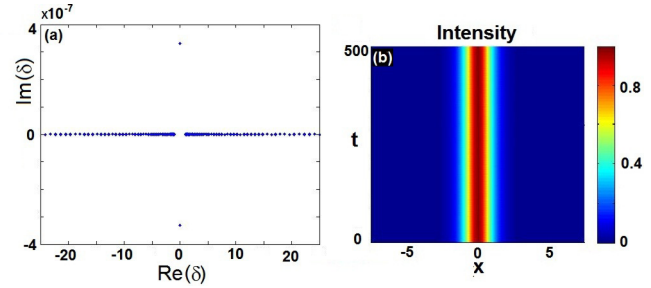

FIG. 5. (Color online) (a) The linear stability eigenvalues; (b) the stable propagation of soliton intensity $|\psi(x,t)|^2$ with $g = -1$. The other parameters are $V_0 = 3$, $W_0 = 0.5$, $k = 1$ (in the region III).

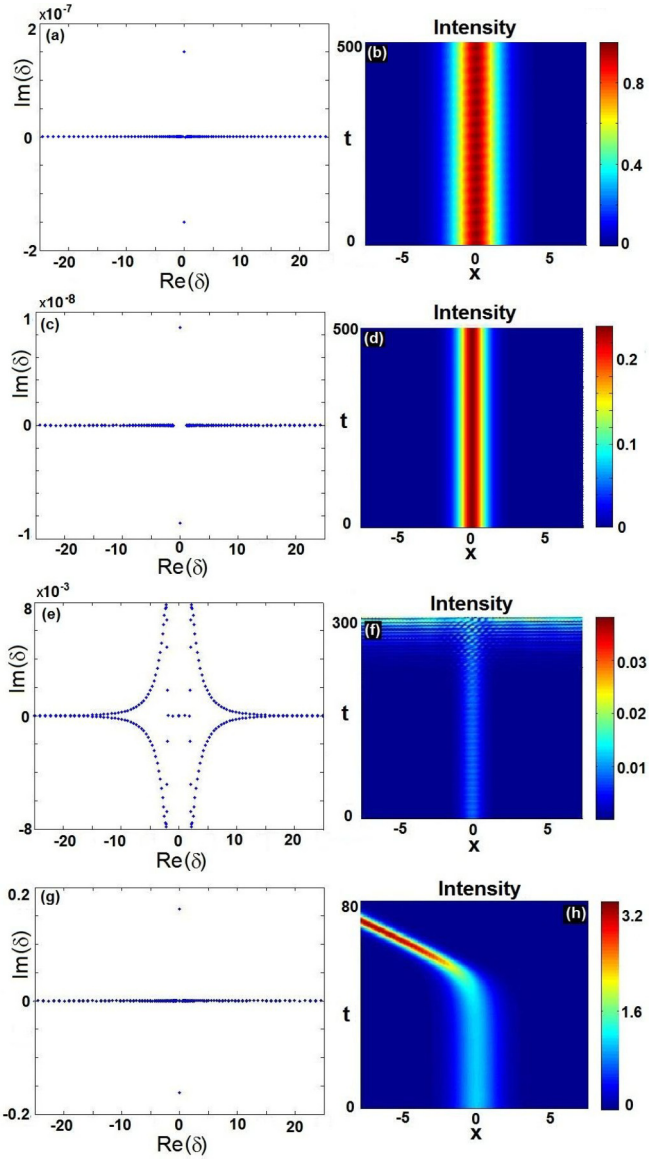

FIG. 6. (Color online) The linear stability eigenvalues (left column) and propagation of soliton intensity $|\psi(x,t)|^2$ with $g=1$ (right column). [(a) and (b)] $V_0=0.05$, $W_0=0.25$, $k=1/\sqrt{2}$ (in region II), [(c) and (d)] $V_0=2.16$, $W_0=0.12$, $k=\sqrt{1.2}$ (in region I_2), [(e) and (f)] $V_0=10$, $W_0=10.4$, $k=\sqrt{2}$ (in region I_1), and [(g) and (h)] $V_0=-0.05$, $W_0=0.05$, $k=1/\sqrt{2}$ (in the region $\{(V_0,W_0)|V_0\leqslant 0, W_0\in\mathbb{R}\}$).

eigenvalues δ [see Fig. 6(e)] and an unstable propagation of the soliton intensity $|\psi(x,t)|^2$ shown in Fig. 6(f); (iv) for $V_0=-0.05$, $W_0=0.05$, $k=1/\sqrt{2}$, in the region $\{(V_0,W_0)|V_0\leqslant 0, W_0\in\mathbb{R}\}$, we numerically obtain the spectrum of eigenvalues δ [see Fig. 6(g)] and an unstable propagation of the soliton intensity $|\psi(x,t)|^2$ shown in Fig. 6(h). If $k\neq 1$ and $g=-1$, for $V_0=6$, $W_0=1$, $k=\sqrt{2}$ in region III (unbroken $\mathcal{PT}$ symmetry), we see that $|\mathrm{Im}(\delta)|=0$ [see Fig. 7(a)] and a stable propagation of the soliton intensity $|\psi(x,t)|^2$ is obtained as shown in Fig. 7(b).

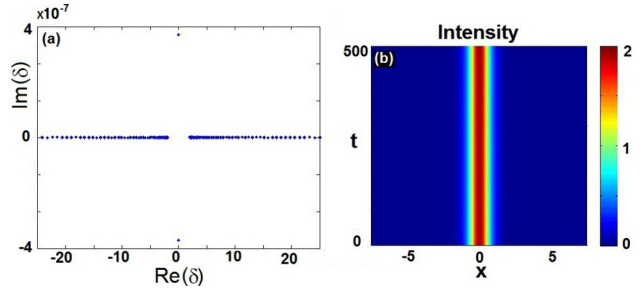

FIG. 7. (Color online) (a) The linear stability eigenvalues; (b) the stable propagation of soliton intensity $|\psi(x,t)|^2$ with $g=-1$. The other parameters are $V_0=6$, $W_0=1$, $k=\sqrt{2}$ (in region III).

C. $\mathcal{PT}$-symmetric multiwell Scarff-II potential

Now we consider another type of $\mathcal{PT}$-symmetric Scarff-II potential, i.e., the $\mathcal{PT}$-symmetric multiwell Scarff-II potential, reading

$$\begin{aligned} V(x) &= \left[\frac{W_0^2}{9}+2-\sigma\cos(\omega x)\right]\mathrm{sech}^2(x),\\ W(x) &= W_0\mathrm{sech}(x)\tanh(x), \end{aligned} \tag{19}$$

where $W_0,\sigma\in\mathbb{R}$ and $\omega\geqslant 0$ denotes the wave number. If $\omega=0$ and $\sigma=W_0^2/9+2-V_0$, then $V(x)$ becomes the usual Scarff-II potential [19,20], which exhibits the shape of a single well, but for nonzero wave number ω, $V(x)$ exhibits the shape of a multiwell, which can provide more abundant structures. For $W_0=0.2$, the external potential $V(x)$ exhibits double-well ($\sigma=2,\omega=1$), single-well ($\sigma=-2,\omega=1$), and multiwell ($\sigma=\pm 2,\omega=6$) structures, respectively (see Fig. 8). In fact, for the fixed parameters W_0 and ω, one can change the parameter σ to control the number of the wells. Note that in the figure we plot the profile of $-V(x)$ because the Hamiltonian of Eq. (1) is $-\partial_x^2-V(x)-iW(x)$. As $\omega\to 0$ (or $\omega\ll 1$), the linear problem associated with the $\mathcal{PT}$-symmetric potential (19) admits an entirely real spectra provided that $|W_0|\leqslant W_0^2/9+9/4-\sigma$. If $\omega\sim 1$, then the condition for the unbroken $\mathcal{PT}$ symmetry is complicated. For the fixed parameter $W_0=0.2$, we find the regions of the unbroken $\mathcal{PT}$ symmetry: (i) $\omega=0.5$, $-550\leqslant\sigma\leqslant 2.5$; (ii) $\omega=1$, $-53.3\leqslant\sigma\leqslant 3.17$; (iii) $\omega=2$, $-13.1\leqslant\sigma\leqslant 6.65$; and (iv) $\omega=5$, $-13.9\leqslant\sigma\leqslant 11.33$.

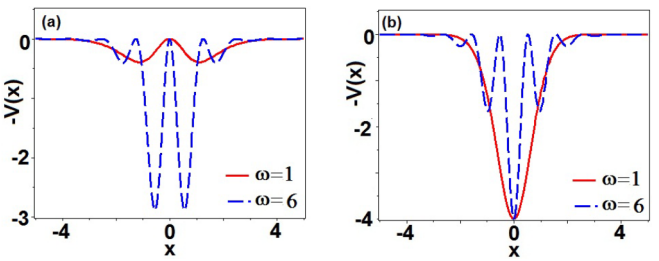

FIG. 8. (Color online) The external potential $-V(x)$ exhibiting a multiwell structure for (a) $\sigma=2$ and (b) $\sigma=-2$. Other parameters are $W_0=0.2$, $\omega=1,6$.

For the $\mathcal{PT}$-symmetric multiwell Scarff-II potential (19), we consider the periodically space-modulated nonlinearity $g \to g(x)$ in Eq. (3) with the form

$$g(x) = \sigma \cos(\omega x). \tag{20}$$

For the zero wave number $\omega = 0$, nonlinearity $g(x)$ is a constant, $g(x) = \sigma$; however, for the given nonzero wave number ω, the nonlinearity $g(x)$ is either positive or negative as x increases. Based on the potential (19) and the nonlinearity (20) we have exact bright solitons of Eq. (3),

$$\phi(x) = \mathrm{sech}(x) e^{i\varphi(x)}, \tag{21}$$

where $\mu = 1$ and the phase is

$$\varphi(x) = \frac{W_0}{3} \arctan[\sinh(x)]. \tag{22}$$

The corresponding transverse power-flow or Poynting vector is given by

$$S(x) = \frac{i}{2}(\phi\phi_x^* - \phi^*\phi_x) = \frac{W_0}{3}\mathrm{sech}^3(x), \tag{23}$$

which implies that $\mathrm{sgn}[S(x)] = \mathrm{sgn}(W_0)$ for any x. Therefore, the power always flows in one direction, i.e., from the gain toward the loss. Moreover, the conserved power is $P(t) = \int_{-\infty}^{+\infty} |\psi(x,t)|^2 = 2$.

Now we consider the linear stability of the soliton solution (21) using Eq. (18) with g being replaced by the periodic function (20) with $W_0 = 0.2$ and different values of ω, σ. We find that for the fixed ω the soliton (21) is more (less) stable if $\sigma < 0$ ($\sigma > 0$). For examples, we show the linear stability eigenvalues and the stable propagation of the soliton (21) for $\omega = 1, \sigma = 2$ [see Figs. 9(a) and 9(b)]; $\omega = 1, \sigma = -2$ [see Figs. 9(c) and 9(d)]; $\omega = 0.5, \sigma = -3$ [see Figs. 9(e) and 9(f)]; and $\omega = 0.5, \sigma = 1$ [see Figs. 9(g) and 9(h)].

For the fixed parameters $W_0 = 0.2, \omega = 0.5$, when $\sigma = -310$, for which the $\mathcal{PT}$ symmetry is unbroken, the soliton (21) is stable [see Fig. 10(b)], however, when $\sigma = 2.5$, in which $\mathcal{PT}$ symmetry is unbroken, the soliton (21) becomes unstable [see Fig. 10(d)]. Thus, for $W_0 = 0.2, \omega = 0.5$, the parameter σ has a significant influence on the linear stability of the soliton solution (21). A negative σ favors obtaining stable solitons.

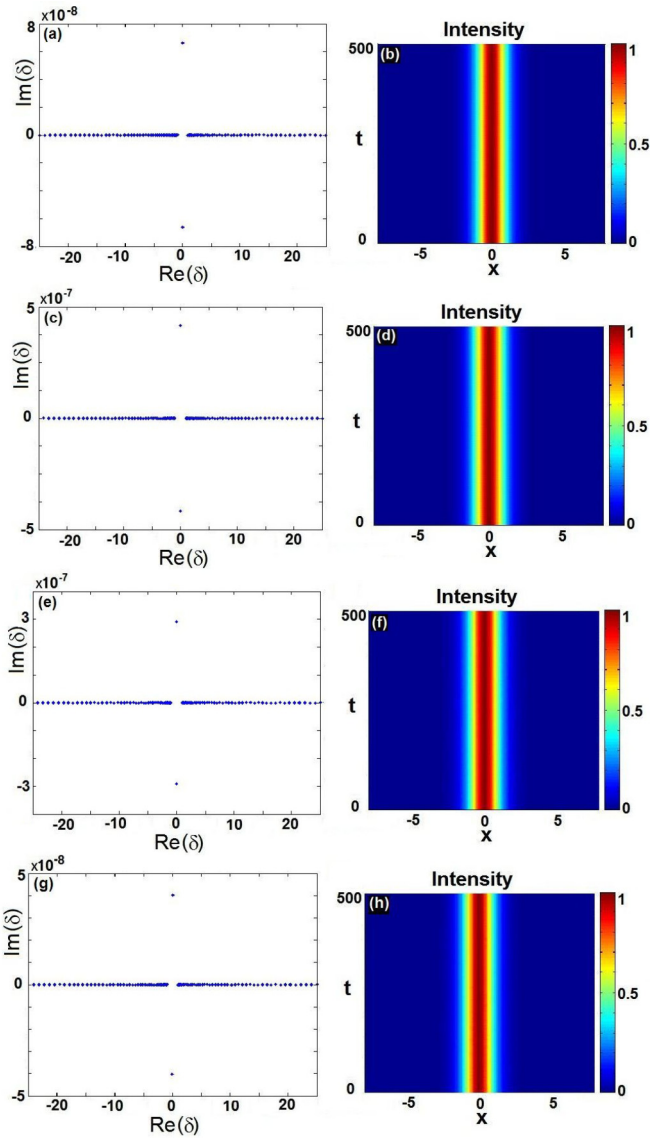

FIG. 9. (Color online) The linear stability eigenvalues (left column) and stable propagation of soliton intensity $|\psi(x,t)|^2$ (right column). [(a) and (b)] $W_0 = 0.2, \omega = 1, \sigma = 2$; [(c) and (d)] $W_0 = 0.2, \omega = 1, \sigma = -2$; [(e) and (f)] $W_0 = 0.2, \omega = 0.5, \sigma = -3$; [(g) and (h)] $W_0 = 0.2, \omega = 0.5, \sigma = 1$. All panels correspond to the unbroken $\mathcal{PT}$ symmetry.

III. SOLITONS IN THREE-DIMENSIONAL $\mathcal{PT}$-SYMMETRIC POTENTIAL

We now consider the 3D NLS equation with the $\mathcal{PT}$-symmetric potential

$$i\partial_t\psi + \nabla^2\psi + [V(x,y,z) + iW(x,y,z)]\psi + g|\psi|^2\psi = 0, \tag{24}$$

where $\psi = \psi(x,y,z,t)$ is a complex field with respect to $x,y,z,t \in \mathbb{R}$, $\nabla^2 = \partial_x^2 + \partial_y^2 + \partial_z^2$, $V(x,y,z)$, and $W(x,y,z)$ are both real-valued functions related to external potential and gain-and-loss distribution, respectively, and g is a real constant with $g = \pm 1$. The $\mathcal{PT}$-symmetric potential requires the sufficient (but not necessary) condition $V(x,y,z) = V(-x,-y,-z)$ and $W(x,y,z) = -W(-x,-y,-z)$. The stationary solution can be solved in the form $\psi(x,y,z) = \phi(x,y,z)e^{i\mu t}$, where μ is the real propagation constant and $\phi(x,y,z)$ satisfies

$$\mu\phi = \nabla^2\phi + [V(x,y,z) + iW(x,y,z)]\phi + g|\phi|^2\phi. \tag{25}$$

We consider the generalized 3D $\mathcal{PT}$-symmetric Scarff-II potential

$$V(x,y,z) = \sum_{\eta=x,y,z}\left(\frac{W_0^2}{9k_\eta^2} + 2k_\eta^2\right)\mathrm{sech}^2(k_\eta\eta) - g\phi_0^2\prod_{\eta=x,y,z}\mathrm{sech}^2(k_\eta\eta), \tag{26}$$

$$W(x,y,z) = W_0\sum_{\eta=x,y,z}\mathrm{sech}(k_\eta\eta)\tanh(k_\eta\eta),$$

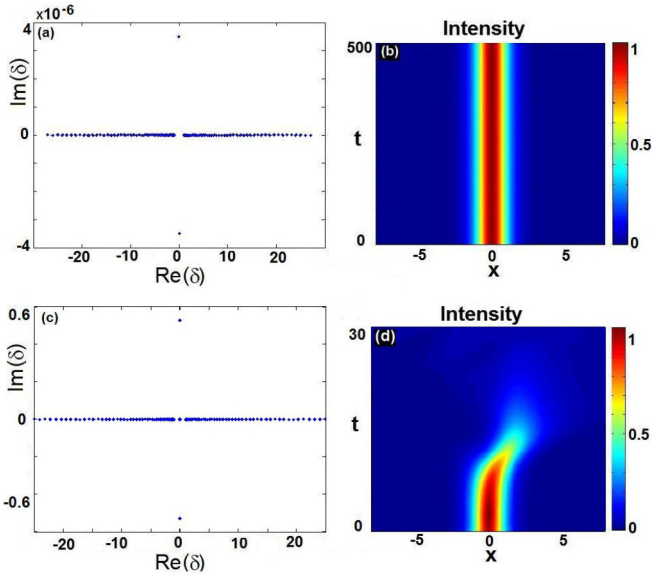

FIG. 10. (Color online) The linear stability eigenvalues (left column) and propagation of soliton intensity $|\psi(x,t)|^2$ (21) (right column). [(a) and (b)] $\sigma = -310$, corresponding to the unbroken $\mathcal{PT}$ symmetry; [(c) and (d)] $\sigma = 2.5$, corresponding to the unbroken $\mathcal{PT}$ symmetry. Other parameters are $W_0 = 0.2$ and $\omega = 0.5$.

where $k_\eta > 0\,(\eta = x,y,z)$ are the wave numbers in the x,y,z directions, respectively, and W_0, ϕ_0 are real constants. In particular, the $\mathcal{PT}$-symmetric potential (26) reduces to the Scarff-II potential (4) when $\eta = x$ and $k_x = 1$. Since x,y,z are symmetric in $V(x,y,z)$ and $W(x,y,z)$ thus we plot their profiles in (x,y) space with $z = 0$ (see Fig. 11). For the self-focusing nonlinearity $g > 0$, the external potential $V(x,y,0)$ exhibits the different profiles as g becomes large [see Figs. 11(a)–11(c)].

For the above-mentioned 3D potential (26) we obtain the exact bright solitons of Eq. (25)

$$\phi(x,y,z) = \phi_0 \mathrm{sech}(k_x x)\mathrm{sech}(k_y y)\mathrm{sech}(k_z z)e^{i\varphi(x,y,z)}, \quad (27)$$

where $\mu = k_x^2 + k_y^2 + k_z^2$ and the phase is

$$\varphi(x,y,z) = \frac{W_0}{3}\sum_{\eta=x,y,z} k_\eta^{-2}\arctan[\sinh(k_\eta \eta)]. \quad (28)$$

The real and imaginary parts and intensity of the solution (27) are shown in Figs. 13(a)–13(c) for $\phi_0 = 1$ and $W_0 = 0.5$.

The velocity field $\mathbf{v}(x,y,z)$ of the solitons (27) have the form

$$\mathbf{v} = \nabla\varphi(x,y,z) = \frac{W_0}{3}\left[k_x^{-1}\mathrm{sech}(k_x x), k_y^{-1}\mathrm{sech}(k_y y), k_z^{-1}\mathrm{sech}(k_z z)\right], \quad (29)$$

which is shown in Fig. 12(a) with $W_0 = 0.5$. It follows from Eq. (29) that the divergence of velocity field $\mathbf{v}(x,y,z)$ (alias the flux density) is given by

$$\mathrm{div}\,\mathbf{v}(\mathrm{x,y,z}) = \nabla\cdot\mathbf{v}(x,y,z) = \nabla^2\varphi(x,y,z) = -\frac{W_0}{3}\sum_{\eta=x,y,z}\mathrm{sech}(k_\eta\eta)\tanh(k_\eta\eta), \quad (30)$$

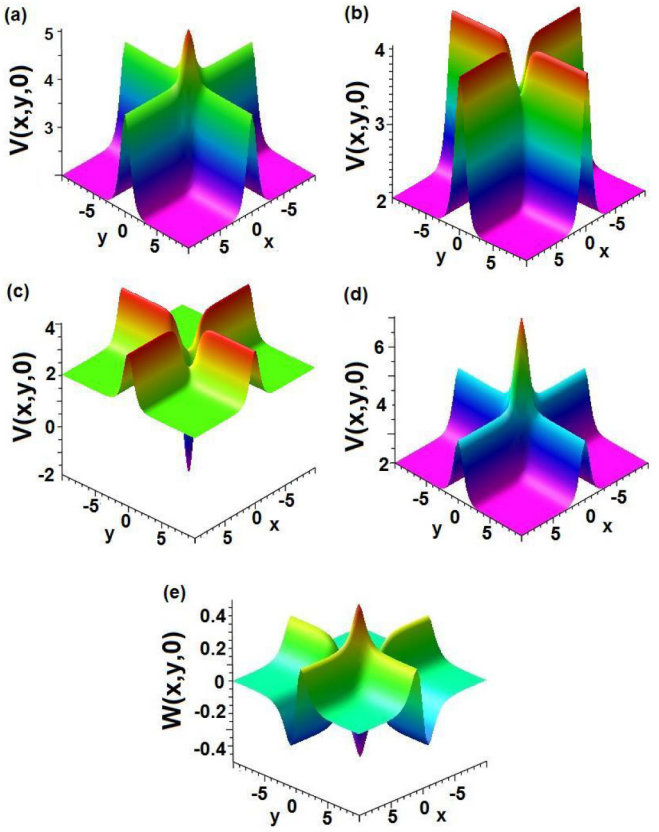

FIG. 11. (Color online) The external potential $V(x,y,0)$ with (a) $g = 1$, (b) $g = 3$, (c) $g = 8$, and (d) $g = -1$; (e) the gain-and-loss distribution $W(x,y,0)$. The parameters are $W_0 = 0.5$ and $\phi_0 = k_x = k_y = k_z = 1$.

which measures the flux per unit area and is dependent on both W_0 and space position. Figure 12(b) shows the flux density in $(x,y,0)$ space. In addition, we also have the relation

$$\mathrm{div}\,\mathbf{v}(x,y,z) = \nabla^2\varphi(x,y,z) = -\tfrac{1}{3}W(x,y,z). \quad (31)$$

From Eq. (30) we have the following proposition. For the given parameter $W_0 > 0$, we have:

(i) the fluid flows outward if $f(x,y,z) < 0$;
(ii) the fluid flows inward if $f(x,y,z) > 0$; and
(iii) the fluid does not flow if $f(x,y,z) = 0$,

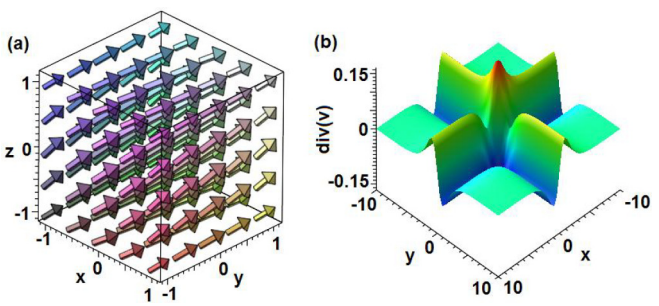

FIG. 12. (Color online) (a) The velocity field $\mathbf{v}(x,y,z)$ (29); (b) the flux density $\mathrm{div}\,\mathbf{v}(x,y,0)$ (30). The parameter are $W_0 = 0.5$ and $k_x = k_y = k_z = 1$.

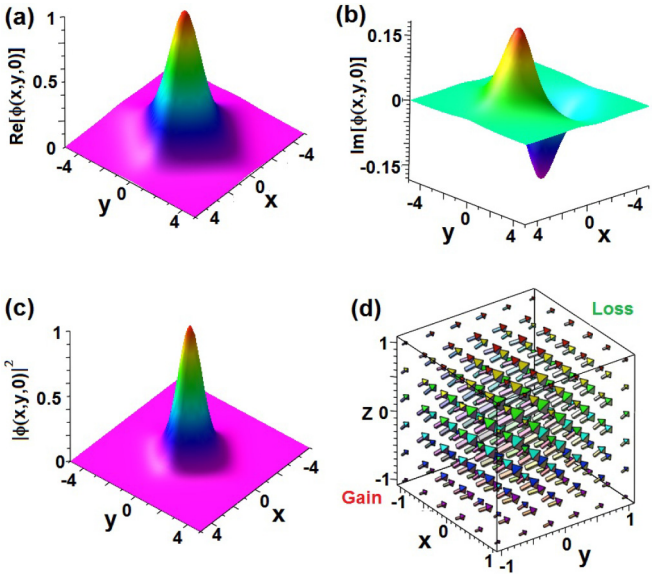

FIG. 13. (Color online) The (a) real part, (b) imaginary part, and (c) the intensity of the soliton solution (27); (d) the transverse power-flow vector (Poynting vector) $\vec{S}(x,y,z)$. The parameter are $W_0 = 0.5$ and $k_x = k_y = k_z = 1$.

where we have introduced $f(x,y,z) = \sum_{\eta=x,y,z} \mathrm{sech}(k_\eta \eta)\tanh(k_\eta \eta)$. For the case $W_0 < 0$, we also have the corresponding results.

For any complex solution $\phi(x,y,z) = |\phi(x,y,z)|e^{i\varphi(x,y,t)}$, we find that its corresponding transverse power-flow or Poynting vector and the gradient of phase obey the relation

$$\vec{S}(x,y,z) = \frac{i}{2}(\phi\nabla\phi^* - \phi^*\nabla\phi) = |\phi(x,y,z)|^2\nabla\varphi(x,y,z). \quad (32)$$

The transverse power-flow or Poynting vector related to the solution (27) is given by

$$\vec{S}(x,y,z) = \phi_0^2 \prod_{\eta=x,y,z} \mathrm{sech}^2(k_\eta\eta)\mathbf{v}(x,y,z) = \frac{W_0\phi_0^2}{3} \prod_{\eta=x,y,z} \mathrm{sech}^2(k_\eta\eta) \times \left[k_x^{-1}\mathrm{sech}(k_x x), k_y^{-1}\mathrm{sech}(k_y y), k_z^{-1}\mathrm{sech}(k_z z)\right], \quad (33)$$

for either $g = 1$ or -1 (i.e., it does not depend on the sign of the nonlinearity), which is exhibited in Fig. 13(d). In addition, the conserved power related to the solution (27) is given by $P(t) = 8\phi_0^2/(k_x k_y k_z)$ for either $g = 1$ or $g = -1$.

IV. CONCLUSION AND DISCUSSION

In conclusion, we have presented a unified theoretical study of the optical bright solitons governed by self-focusing and defocusing NLS equations with $\mathcal{PT}$-symmetric Scarff-II-like potentials. Particularly, a $\mathcal{PT}$-symmetric k-wave-number Scarff-II potential and a multiwell Scarff-II potential are considered, respectively. For the k-wave-number Scarff-II potential, the parameter space can be divided into different regions, corresponding to unbroken and broken $\mathcal{PT}$ symmetry and bright solitons with self-focusing and defocusing Kerr nonlinearities. For the multiwell Scarff-II potential the bright solitons can be obtained by using a periodically space-modulated Kerr nonlinearity. The linear stability of bright solitons with $\mathcal{PT}$-symmetric k-wave-number and multiwell Scarff-II potentials is analyzed in detail by using numerical simulations. Stable and unstable bright solitons are found in both regions of unbroken and broken $\mathcal{PT}$ symmetry due to the existence of the nonlinearity. Furthermore, the bright solitons in 3D self-focusing and defocusing NLS equations with a generalized $\mathcal{PT}$-symmetric Scarff-II potential are explored. The used method can also be used to study optcial solitons in other $\mathcal{PT}$-symmetric k-wave-number potentials.

The results we obtained in this work provide a new way of control over soliton stability by using generalized $\mathcal{PT}$-symmetric Scarff-II potentials in different parameter domains. This may have potential applications in the field of optical information transmission and processing based on optical solitons in nonlinear dissipative but $\mathcal{PT}$-symmetric systems.

ACKNOWLEDGMENTS

The authors thank the referees for their invaluable suggestions. The work of Z.Y.Y. and Z.C.W. was partially supported by NSF-China under Grant No. 61178091, NKBRPC under Grant No. 2011CB302400, and the Open Project Program of State Key Laboratory of Theoretical Physics, Institute of Theoretical Physics, Chinese Academy of Sciences, China under Grant No. Y4KF211CJ1. The work of C.H. was supported by NSF-China under Grant No. 11475063.

[1] M. J. Ablowitz and P. A. Clarkson, *Solitons, Nonlinear Evolution Equations and Inverse Scattering* (Cambridge University Press, Cambridge, 1991).
[2] C. Sulem and P. L. Sulem, *The Nonlinear Schrödinger Equation: Self-focusing and Wave Collapse* (Springer-Verlag, New York, 1999).
[3] Y. S. Kivshar and G. P. Agrawal, *Optical Solitons: From Fibers to Photonic Crystals* (Academic Press, San Diego, CA, 2003).
[4] G. P. Agrawal, *Nonlinear Fiber Optics*, 3rd ed. (Academic Press, San Diego, CA, 2001).
[5] A. Hasegawa and M. Matsumoto, *Optical Solitons in Fibers* (Springer, Berlin, 2003).
[6] V. E. Zakharov and A. B. Shabat, Sov. Phys JETP **34**, 62 (1972).
[7] V. E. Zakharov and A. B. Shabat, Sov. Phys. JETP **37**, 823 (1973).
[8] S. P. Novikov, S. V. Manakov, L. P. Pitaevskii, and V. E. Zakharov, *Theory of Solitons. The Inverse Scattering Method* (Plenum, New York, 1984).
[9] L. Pitaevskii and S. Stringari, *Bose-Einstein Condensation* (Oxford University Press, Oxford, 2003).

[10] C. J. Pethick and H. Smith, *Bose-Einstein Condensation in Dilute Gases* (Cambridge University Press, Cambridge, 2002).

[11] R. Carretero-González, D. J. Frantzeskakis, and P. G. Kevrekidis, Nonlinearity **21**, R139 (2008).

[12] Y. V. Kartashov, B. A. Malomed, and L. Torner, Rev. Mod. Phys. **83**, 247 (2011).

[13] J. Belmonte-Beitia, V. M. Pérez-Garcia, V. Vekslerchik, and P. J. Torres, Phys. Rev. Lett. **98**, 064102 (2007).

[14] Z. Y. Yan, Phys. Lett. A **374**, 672 (2010); **374**, 4838 (2010).

[15] Z. Y. Yan and D. M. Jiang, Phys. Rev. E **85**, 056608 (2012); Z. Y. Yan and V. V. Konotop, *ibid.* **80**, 036607 (2009); Z. Y. Yan, Nonlinear Dyn. **79**, 2515 (2015); Y. Q. Yang, Z. Y. Yan, and D. Mihalache, J. Math. Phys. **56**, 053508 (2015).

[16] S. A. Ponomarenko and G. P. Agrawal, Phys. Rev. Lett. **97**, 013901 (2006).

[17] V. N. Serkin, A. Hasegawa, and T. L. Belyaeva, Phys. Rev. Lett. **98**, 074102 (2007).

[18] C. M. Bender and S. Boettcher, Phys. Rev. Lett. **80**, 5243 (1998); C. M. Bender, Rep. Prog. Phys. **70**, 947 (2007).

[19] G. Lévai and M. Znojil, J. Phys. A **33**, 7165 (2000).

[20] Z. Ahmed, Phys. Lett. A **282**, 343 (2001).

[21] Z. H. Musslimani, K. G. Makris, R. El-Ganainy, and D. N. Christodoulides, Phys. Rev. Lett. **100**, 030402 (2008).

[22] Z. H. Musslimani *et al.*, J. Phys. A **41**, 244019 (2008).

[23] Y. Lumer, Y. Plotnik, M. C. Rechtsman, and M. Segev, Phys. Rev. Lett. **111**, 263901 (2013).

[24] Z. Shi, X. Jiang, X. Zhu, and H. Li, Phys. Rev. A **84**, 053855 (2011).

[25] F. K. Abdullaev, Y. V. Kartashov, V. V. Konotop, and D. A. Zezyulin, Phys. Rev. A **83**, 041805(R) (2011).

[26] S. Nixon, L. Ge, and J. Yang, Phys. Rev. A **85**, 023822 (2012).

[27] D. A. Zezyulin and V. V. Konotop, Phys. Rev. A **85**, 043840 (2012).

[28] Z. Y. Yan *et al.*, arXiv:1009.4023; Z. Y. Yan, Phil. Trans. R. Soc. A **371**, 20120059 (2013).

[29] B. Midya and R. Roychoudhury, Phys. Rev. A **87**, 045803 (2013).

[30] S. Hu, X. Ma, D. Lu, Z. Yang, Y. Zheng, and W. Hu, Phys. Rev. A **84**, 043818 (2011).

[31] V. Achilleos, P. G. Kevrekidis, D. J. Frantzeskakis, and R. Carretero-Gonzalez, Phys. Rev. A **86**, 013808 (2012).

[32] C. H. Tsang, B. A. Malomed, and K. W. Chow, Phys. Rev. E **84**, 066609 (2011).

[33] F. K. Abdullaev, V. V. Konotop, M. Salerno, and A. V. Yulin, Phys. Rev. E **82**, 056606 (2010).

[34] K. Li and P. G. Kevrekidis, Phys. Rev. E **83**, 066608 (2011).

[35] S. V. Suchkov, B. A. Malomed, S. V. Dmitriev, and Y. S. Kivshar, Phys. Rev. E **84**, 046609 (2011).

[36] D. A. Zezyulin and V. V. Konotop, Phys. Rev. Lett. **108**, 213906 (2012).

[37] V. E. Lobanov, O. V. Borovkova, and B. A. Malomed, Phys. Rev A **90**, 053820 (2014).

[38] J. K. Yang, Phys. Rev. E **91**, 023201 (2015).

[39] The Scarff potential is given by $V_0\mathrm{sech}^2(x) + W_0\mathrm{sech}(x)\tanh(x)$ with $V_0, W_0 \in \mathbb{R}$. The extension of the Scarff potential in the complex space is ususally called the Scarff-II potential, which is written as $V_0\mathrm{sech}^2(x) + iW_0\mathrm{sech}(x)\tanh(x)$ with $V_0, W_0 \in \mathbb{R}$.

[40] Z. C. Wen and Z. Y. Yan, Phys. Lett. A **379**, 2025 (2015).

[41] Z. Y. Yan, Z. C. Wen, and V. V. Konotop, Phys. Rev. A **92**, 023821 (2015).

[42] Z. Y. Yan, Appl. Math. Lett. **47**, 61 (2015).

[43] A. Guo, G. J. Salamo, D. Duchesne, R. Morandotti, M. Volatier-Ravat, V. Aimez, G. A. Siviloglou, and D. N. Christodoulides, Phys. Rev. Lett. **103**, 093902 (2009).

[44] L. Feng, M. Ayache, J. Huang, Y.-L. Xu, M.-H. Lu, Y.-F. Chen, Y. Fainman, and A. Scherer, Science **333**, 729 (2011).

[45] A. Regensburger, C. Bersch, M.-A. Miri, G. Onishchukov, D. N. Christodoulides, and U. Peschel, Nature (London) **488**, 167 (2012).

[46] C. Hang, G. Huang, and V. V. Konotop, Phys. Rev. Lett. **110**, 083604 (2013).

[47] J. Sheng, M. A. Miri, D. N. Christodoulides, and M. Xiao, Phys. Rev. A **88**, 041803(R) (2013).

[48] C. Hang, D. A. Zezyulin, V. V. Konotop, and G. Huang, Opt. Lett. **38**, 4033 (2013).

[49] C. Hang, D. A. Zezyulin, G. Huang, V. V. Konotop, and B. A. Malomed, Opt. Lett. **39**, 5387 (2014).

[50] C. Hang and G. Huang, Phys. Rev. A **91**, 043833 (2015).

[51] B. Peng *et al.*, Nat. Phys. **10**, 394 (2014).

[52] L. Chang *et al.*, Nat. Photon. **8**, 524 (2014).

[53] M. Znojil, J. Phys. A **33**, L61 (2000).

[54] The family of k-wave-number open rays l_1: $W_0 = V_0 + k^2/4 (V_0 > 0)$ and the family of k-wave-number parabolas l_3: $W_0^2 = 9k^2(V_0 - 2k^2)(V_0 > 2k^2)$ have only one crossover point $P_1 = (17k^2/4, 9k^2/2)$, i.e., the open ray l_1 is tangent to the parabola l_3 at the point P_1. Similarly, another family of k-wave-number open rays l_2: $W_0 = -(V_0 + k^2/4)(V_0 > 0)$ is also tangent to the parabola l_3 at the point $P_2 = (17k^2/4, -9k^2/2)$.

[55] E. A. Kuznetsov, A. M. Rubenchik, and V. E. Zakharov, Phys. Rep. **142**, 103 (1986).